VRX Wind

Brian Bingham
Naval Postgraduate School

June 4, 2020

1 Environment Modeling

A key aspect of extending the Gazebo robotics simulator to support ocean robotics is the ability to represent the influence of the ocean environment on the robotic system. For USV applications the most important environmental influences are waves and wind.

VRX uses a model-based approach where the models are based on spectral representations of the stochastic wave and wind environments. Empirical environmental models are described as power spectral density (PSD) representations. We adopt spectral representation methods [Shinozuka and Deodatis, 1991] to generate time series realizations of the stochastic process with the prescribed PSD. Because wind and wave environments are often characterized by power spectra, this approach allows simulations to be tied directly to standard ocean environments with mature descriptions from oceanography.

1.1 Wind Modeling

Wind is a significant disturbance for objects at the sea surface. We consider the total wind speed $V_w(t)$ consisting of the sum of the constant mean wind speed ($\bar{v}$) and stochastic, zero-mean, variable wind speed ($v_g(t)$) due to turbulence and gusting, i.e., $V_w(t) = \bar{v} + v_g(t)$.

Spectral representations of ocean wind environments are common and generally model the variable component of wind speed as a wide-sense stationary, Gaussian stochastic process. Typical models of wind over water include Harris [1971], Forristall [1988] and Ochi and Shin [2013]. Cole [2018] showed that the Forristall and Ochi and Shin models are in agreement, while the Harris model underestimates the spectral content. While the implementation is not specific to any one spectral model of stochastic wind, for illustration purposes we use the Forristall wind spectra. The form of the one-sided spectra is Olesen et al. [1984] blunt model for micrometeorology, where Forristall showed that normalizing the one-sided spectrum by the variance (σ) produced improved experimental agreement:

$$\widetilde{S}_f(f) = \frac{S_f(f)\, f}{\sigma^2} = \frac{A f^*}{(1 + B f^*)^{5/3}}. \tag{1}$$

In this dimensionless form f is the oscillation frequency in Hz and f^* is the standard nondimenstional frequency from atmospheric boundary layer studies,

$$f^* = \frac{f\, z}{\bar{v}(z)}, \tag{2}$$

where z is the height and $\bar{v}(z)$ is the mean wind speed as a function of height. The constants A and B are chosen to fit specific observational data. We use the mean coefficients from of $A = 42.0$ and $B = 63.0$, as reported by Forristall [1988] These values satisfy the constraint $A = (2/3)B$, necessary so that the variance of the stochastic process is σ^2, i.e.,

$$\int_0^\infty S_f(f)df = \sigma^2. \tag{3}$$

The Forristall normalized spectrum is illustrated in Figure 1. The peak of the spectrum (1) occurs at

$$f_p^* = \frac{3}{2B}. \tag{4}$$

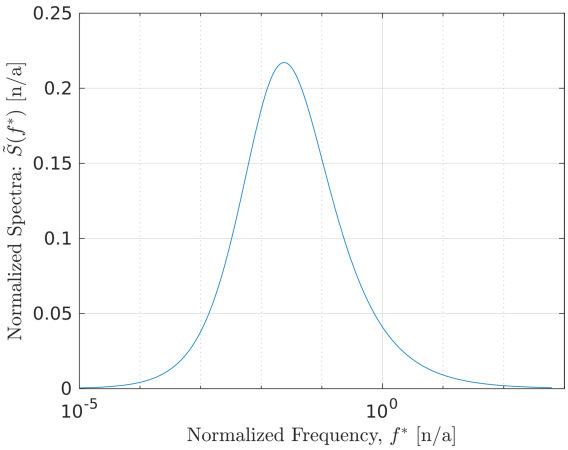

Figure 1: Forristall normalized spectrum.

For generating physically meaningful wind time series simulations it is necessary to take into account the physical dimesions of the spectra. We consider a constant height of $z = 10\,\mathrm{m}$ and mean wind velocity at that height $\bar{v}(z = 10) = \bar{v}_{10}$. Figure 2 illustrates how mean wind speed affects the generated spectra. The cutoff frequency f_c for the dimensional spectra is the frequency for which $S_f(f_c) = 0.5S_f(0)$. In dimensionless and dimensional forms, the cutoff frequency is

$$f_c^* = \frac{2^{3/5} - 1}{B} \tag{5}$$

$$f_c = \frac{(2^{3/5} - 1)\bar{v}(z)}{B\, z} \tag{6}$$

$$= (8.19 \times 10^{-4})\, \bar{v}_{10} \tag{7}$$

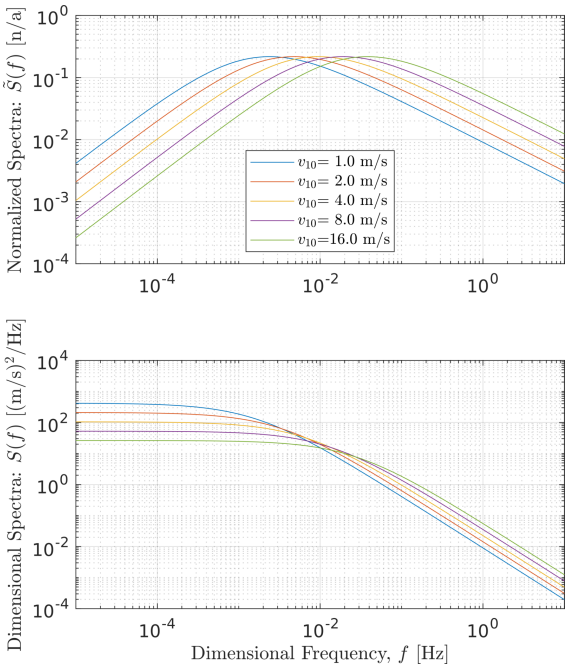

Figure 2: Dimensional Forristall spectra with unit variance.

1.1.1 Wind speed variance

In the Forristall model the variance of the wind speed is not a simple function of the mean wind speed. The ratio of the variance to the friction velocity (v_*) can be approximated as

$$\frac{\sigma}{v_*} = 3.0w \tag{8}$$

where w is determined from the predicted ocean significant wave height H_n and the observed significant wave height H_s as

$$w = 1 + \frac{H_s - H_n}{2H_n}. \tag{9}$$

For the purposes of this example, we consider a developed sea where $H_s = H_n$.

The friction velocity is determined by using the logarithmic boundary layer mean velocity profile

$$\bar{v}(z) = \frac{v_*}{\kappa} \ln\left(\frac{z}{z_0}\right) \tag{10}$$

where the von Karman's constant is $\kappa = 0.41$ and z_0 is the sea surface roughness. It is common to re-write (10) at a reference altitude of $z = 10\,\mathrm{m}$ and solve for the friction velocity

$$v_* = \frac{\kappa\,\bar{v}(z=10)}{\ln(z=10/z_0)} = \frac{\kappa\,\bar{v}_{10}}{\ln(10/z_0)}. \tag{11}$$

Multiple models of the relationship between sea surface roughness (z_0) and friction velocity (v_*) are available. Based on dimensional analysis Charnock [1955] proposed

$$\frac{z_0 g}{v_*^2} = \alpha \tag{12}$$

where g is the acceleration of gravity; $\alpha = [0.013, 0.0185]$ has been found to be consistent with empirical wind profiles over the ocean [Garratt, 1977, Toba et al., 1990].

Without loss of generality, we numerically solve for V_* by combining (11) and (12) with $\alpha = 0.0144$ for values of $v_{10} = [4, 21]\mathrm{m/s}$ [Garratt, 1977]. The resulting values are illustrated in Figure 3. To simplify

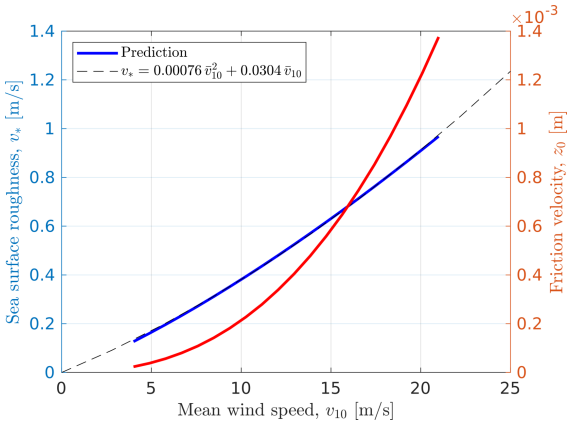

Figure 3: Sea surface roughness and friction velocity as a function of mean wind speed.

the implementation, we fit a quadratic polynomial to the sea surface roughness prediction via nonlinear regression, enforcing that the y-intercept be zero. The resulting relationship, also shown in Figure 3, is

$$v_* = 0.00076\,\bar{v}_{10}^2 + 0.0304\,\bar{v}_{10} \tag{13}$$

which allows expression of the wind speed variance as a function of mean wind speed,

$$\sigma^2 = \left[3\,w(0.00076\,\bar{v}_{10}^2 + 0.0304\,\bar{v}_{10})\right]^2. \tag{14}$$

Substituting (1) and the constants described above into (14) allows us to express the dimensional Forristall spectrum for wind speed at $z = 10.0\,\mathrm{m}$ altitude as a function of only the mean wind speed,

$$S_f(f) = \left[3\,(0.00076\,\bar{v}_{10}^2 + 0.0304\,\bar{v}_{10})\right]^2 \frac{(42.0)10.0/\bar{v}_{10}}{\left(1 + \frac{63.0(10.0)f}{\bar{v}_{10}}\right)^{5/3}}. \tag{15}$$

1.1.2 Generating Wind Time Series

The wind model is described by the PSD in (15) which allows us to generate sample functions of the underlying stochastic process using a summation of cosines approach similar to the implementation of the Gerstner waves. The combined turbulence and gusting wind speed is expressed as

$$v_g(t) = \sqrt{2} \sum_{n=0}^{M-1} A_n \cos(\omega_n t + \phi_n) \tag{16}$$

where

$$A_n = \left(\frac{1}{2\pi} S_f(f_n = \omega_n/(2\pi)) \Delta\omega \right)^{1/2}, \tag{17a}$$

$$\omega_n = n\Delta\omega, \ n = 0, 1, 2, ..., N-1 \tag{17b}$$

$$\Delta\omega = \omega_u / M. \tag{17c}$$

The frequency sampling is $\Delta\omega$, the upper cut-off frequency, ω_u, is the frequency beyond which the PSD may be assumed to be zero, $\phi_0, \phi_1, ..., \phi_{M-1}$ are random phase angles distributed uniformly over the interval $[0, 2\pi)$. Note the factor of $1/(2\pi)$ in (17a) is necessary to maintain the integral relationship between the spectrum and the variance of the underlying stochastic process, i.e.,

$$E[v_g^2(t)] = \sigma_{v_g}^2 \tag{18a}$$

$$= \int_0^\infty S_f(f) df \tag{18b}$$

$$= \frac{1}{2\pi} \int_0^\infty S_f(f = \frac{\omega}{2\pi}) d\omega \tag{18c}$$

$$\leq \frac{1}{2} \left(\frac{2\pi}{\Delta\omega} \right) \frac{1}{M}. \tag{18d}$$

The condition

$$A_0 = 0 \text{ or } S_f(\omega_0 = 0) = 0 \tag{19}$$

is necessary and must be forced if $S_{yy}(0) \neq 0$. The resulting simulated time series is periodic with period

$$T_0 = \frac{2\pi}{\Delta\omega}. \tag{20}$$

By combining (15), (16) and (17) we are able to generate a physically relevant time series realization, v_g, of the variable wind speed stochastic process described by the Forristall wind spectrum. For wind at $z = 0$ and a fully developed sea ($H_s = H_n$) this time series is solely a function of mean wind speed, $\bar{v} = v_{10}$. The example in Figure 4 illustrates the results for three different mean wind speeds. In the upper axis, the speed is normalized by the standard deviation of the time series to illustrate the similarity in the results. This view also highlights that the higher mean wind velocities generate spectra with a slightly higher cutoff frequency (5).

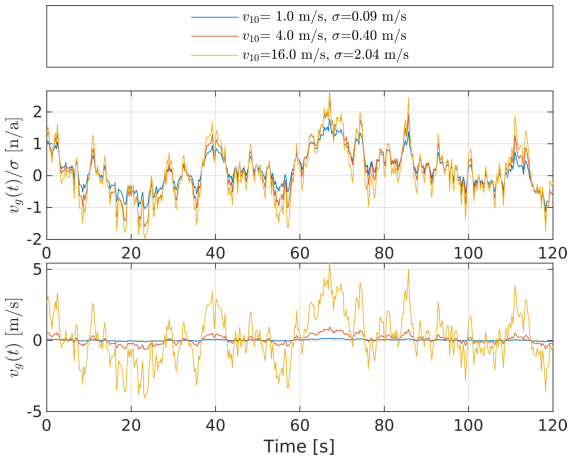

Figure 4: Example time series of variable wind speed component generated by spectral representation for Forristall spectrum for different mean wind speed values.

1.2 Wind Forces

The model used for simulating the wind environment—consisting of horizontal wind speed (V_w) and direction (β_w)—is described in Section 1.1. We consider the influence of this wind on the maneuvering degrees-of-freedom of the model. We neglect the wind-induced motion in heave, pitch and roll. While the influence on heave and pitch are typically very small, for certain vessels, under certain conditions, the wind can have an effect on roll. For such cases the same coefficient-based model presented below can be extended.

We adapt the model and notation described by Fossen [1994]. The relative (apparent) wind velocities are

$$u_{rw} = u - u_w \tag{21a}$$

$$v_{rw} = v - v_w \tag{21b}$$

where u_w and v_w are the x and y components of the simulated wind velocity in the vessel body frame, expressed as

$$u_w = V_w \cos(\beta_w - \psi) \tag{22a}$$

$$v_w = V_w \sin(\beta_w - \psi). \tag{22b}$$

The surge, sway and yaw components of the wind force vector ($\boldsymbol{\tau}_{wind}$ in (**??**)) are dependent upon the apparent wind and the coefficients for each mode. For symmetrical vessels, these wind coefficients can be

considered constant. Using dimensional wind coefficients $\bar{c}_x$, $\bar{c}_y$ and $\bar{c}_n$ we express the forcing terms as

$$X_{wind} = \bar{c}_x u_{rw} |u_{rw}| \tag{23a}$$

$$Y_{wind} = \bar{c}_y v_{rw} |v_{rw}| \tag{23b}$$

$$N_{wind} = -2.0 \bar{c}_n u_{rw} v_{rw}. \tag{23c}$$

This wind forcing model is implemented as another standalone Gazebo plugin. At runtime the user specifies the wind characteristics—mean direction and speed—and the vessel-specific wind coefficients in (23). The wind speed and direction at simulation time is calculated according to the wind generation model in (17), the components of the apparent wind are calculated in the vessel body-frame and the resulting forces from (23) are applied to the simulated vessel for inclusion in the next cycle of the physics engine update.

Analogous to the hydrodynamic model, this approach to representing wind-induced forces is generally applicable to surface vessels and a vessel-specific application requires estimation of the wind coefficients. For the WAM-V model, wind coefficients have been estimated based on experimental testing [Sarda et al., 2016]. We use these numerical values for the WAM-V for the purposes of the VRX challenge reference implementation.

References

Masanobu Shinozuka and George Deodatis. Simulation of Stochastic Processes by Spectral Representation. *Applied Mechanics Reviews*, 44(4):191–204, 04 1991. ISSN 0003-6900. doi: 10.1115/1.3119501. URL `https://doi.org/10.1115/1.3119501`.

R. I. Harris. The nature of the wind, the modern design of wind-sensitive structures. In *Construction Industry Research and Information Association*, pages 29–55, 1971.

George Z. Forristall. Wind spectra and gust factors over water. In *Proc. 20th Offshore Technology Conference*, 1988.

M.K. Ochi and V.S. Shin. Wind turbulent spectra for design consideration of offshore structures. In *Offshore Technology Conference*, 04 2013.

Kenneth Cole. *Reactive Trajectory Generation and Formation Control for Groups of UAVs in Windy Environments*. PhD thesis, The George Washington University, 2018.

H.R. Olesen, S. E. Larsen, and J. Hjstrup. Modelling velocity spectra in the lower part of the planetary boundary layer. *Boundary-Layer Meteorology*, 1984.

H. Charnock. Wind stress on a water surface. *Quarterly Journal of the Royal Meteorological Society*, 81(350): 639–640, 1955. doi: 10.1002/qj.49708135027. URL `https://rmets.onlinelibrary.wiley.com/doi/abs/10.1002/qj.49708135027`.

J. R. Garratt. Review of drag coefficients over oceans and continents. *Monthly Weather Review*, 105(7): 915–929, 1977. doi: 10.1175/1520-0493(1977)105⟨0915:RODCOO⟩2.0.CO;2. URL https://doi.org/10.1175/1520-0493(1977)105<0915:RODCOO>2.0.CO;2.

Yoshiaki Toba, Noriko Iida, Hiroshi Kawamura, Naoto Ebuchi, and Ian S. F. Jones. Wave dependence of sea-surface wind stress. *Journal of Physical Oceanography*, 20(5):705–721, 1990. doi: 10.1175/1520-0485(1990)020⟨0705:WDOSSW⟩2.0.CO;2. URL https://doi.org/10.1175/1520-0485(1990)020<0705:WDOSSW>2.0.CO;2.

Thor I. Fossen. *Guidance and Control of Ocean Vehicles*. Wiley, 1994.

Edoardo I. Sarda, Huajin Qu, Ivan R. Bertaska, and Karl D. von Ellenrieder. Station-keeping control of an unmanned surface vehicle exposed to current and wind disturbances. *Ocean Engineering*, 127:305 – 324, 2016. ISSN 0029-8018.